Original Article

http://dx.doi.org/10.3349/ymj.2015.56.3.726
pISSN: 0513-5796, eISSN: 1976-2437

Yonsei Med J 56(3):726-736, 2015

YMJ

A Network Analysis of ^{15}O-H_2O PET Reveals Deep Brain Stimulation Effects on Brain Network of Parkinson's Disease

Hae-Jeong Park,[1,2] Bumhee Park,[1] Hae Yu Kim,[3] Maeng-Keun Oh,[1] Joong Il Kim,[1,2] Misun Yoon,[1,2] Jong Doo Lee,[1,2] and Jin Woo Chang[2,3]

Departments of [1]Nuclear Medicine and [3]Neurosurgery, Yonsei University College of Medicine, Seoul; [2]BK21 PLUS Project for Medical Science, Yonsei University College of Medicine, Seoul, Korea.

Received: May 7, 2014
Revised: July 1, 2014
Accepted: July 11, 2014
Corresponding author: Dr. Jin Woo Chang, Department of Neurosurgery, Yonsei University College of Medicine, 50-1 Yonsei-ro, Seodaemun-gu, Seoul 120-752, Korea.
Tel: 82-2-2228-2159, Fax: 82-2-312-0578
E-mail: jchang@yuhs.ac

· The authors have no financial conflicts of interest.

Purpose: As Parkinson's disease (PD) can be considered a network abnormality, the effects of deep brain stimulation (DBS) need to be investigated in the aspect of networks. This study aimed to examine how DBS of the bilateral subthalamic nucleus (STN) affects the motor networks of patients with idiopathic PD during motor performance and to show the feasibility of the network analysis using cross-sectional positron emission tomography (PET) images in DBS studies. **Materials and Methods:** We obtained [^{15}O]H_2O PET images from ten patients with PD during a sequential finger-to-thumb opposition task and during the resting state, with DBS-On and DBS-Off at STN. To identify the alteration of motor networks in PD and their changes due to STN-DBS, we applied independent component analysis (ICA) to all the cross-sectional PET images. We analysed the strength of each component according to DBS effects, task effects and interaction effects. **Results:** ICA blindly decomposed components of functionally associated distributed clusters, which were comparable to the results of univariate statistical parametric mapping. ICA further revealed that STN-DBS modifies usage-strengths of components corresponding to the basal ganglia-thalamo-cortical circuits in PD patients by increasing the hypoactive basal ganglia and by suppressing the hyperactive cortical motor areas, ventrolateral thalamus and cerebellum. **Conclusion:** Our results suggest that STN-DBS may affect not only the abnormal local activity, but also alter brain networks in patients with PD. This study also demonstrated the usefulness of ICA for cross-sectional PET data to reveal network modifications due to DBS, which was not observable using the subtraction method.

Key Words: Deep brain stimulation, brain networks, Parkinson's disease, H_2O PET, independent component analysis

© Copyright:
Yonsei University College of Medicine 2015

This is an Open Access article distributed under the terms of the Creative Commons Attribution Non-Commercial License (http://creativecommons.org/licenses/by-nc/3.0) which permits unrestricted non-commercial use, distribution, and reproduction in any medium, provided the original work is properly cited.

INTRODUCTION

The mechanisms by which deep brain stimulation (DBS) of the subthalamic nucleus (STN) modifies behaviour or performance of patients with Parkinson's disease (PD) have been investigated in a number of positron emission tomography (PET) studies. For the abnormal brain involvement during motor tasks in patients

with PD,[1-3] STN-DBS promotes task-specific modifications by increasing activities in hypoactive regions, while decreasing those in hyperactive regions.[1,4] However, the effects of DBS on motor tasks have mostly been investigated in the aspect of regional changes, rather than changes in networks. Therefore, it is not fully understood how STN-DBS affects the functional networks for motor tasks in patients with PD.

Despite its importance, investigation of the DBS effect on the brain network of PD was hampered by the method to explore functional connectivity among brain regions during DBS. Although resting state functional magnetic resonance imaging (fMRI) makes it possible to research functional connectivity in patients with PD,[5,6] it is not a simple matter to directly apply this method to a DBS study in a conventional way due to safety issues of fMRI. PET imaging, preferably used in many DBS studies, does not provide time-series information to estimate functional connectivity, defined in the fMRI or electroencephalogram domain. Thus, an alternative approach is needed to estimate DBS-induced network alterations using PET images.

To explore brain networks using static PET images, correlation or covariance structures in cross-sectional PET images have been used.[7-10] For example, the principal component analysis (PCA), a most representative method in the covariance approach, estimates spatially 'orthogonal' components that represent functional association among brain regions.[11] However, in exploring hidden source components constructing diverse brain activities, source components may be more plausibly modeled with mutually 'independent' activation patterns than mutually 'orthogonal' patterns posited in PCA. For this reason, Park, et al.[12] introduced an independent component analysis (ICA), a well-established method in the fMRI analysis,[13-15] to cross-sectional PET image analysis and showed that ICA can be reliably used to decompose mutually 'independent' spatial components common to all subjects or tasks.

To understand the effects of DBS on motor networks in patients with advanced PD, we propose an ICA analysis of ^{15}O-H_2O PET images during a motor performance of patients with DBS-On and DBS-Off. In order to measure different brain states between DBS-On and Off within several hours, we used ^{15}O-H_2O PET imaging because of its shorter half-life (2.07 minutes) than other nuclear medicine imaging approaches such as ^{18}F-fluorodeoxyglucose-PET (110 minutes) or Technetium-99m HMPAO single photon emission tomography (6.03 hours).

We hypothesized that STN-DBS would modify functional networks during a motor performance in patients with PD, and this would be reflected in the use of functional components driven by ICA. Consequently, this experiment aimed to establish whether cross-sectional ICA of PET images could be used as a measure for identifying alterations in the functional networks due to STN-DBS in patients with PD, which were but are not made evident with the subtraction method.

MATERIALS AND METHODS

Subjects

Ten right-handed patients (four males and six females) diagnosed with idiopathic PD and treated with bilateral STN-DBS were enrolled in this study. Their symptomatic dominance was right:left=5:5. The mean age at disease onset was 48.6 (±9.83) years, while the mean age at surgery was 58.1 (±8.97) years and the mean age at scan was 61.0 (±7.97) years. The mean interval between DBS surgery and PET scanning was 32.8 months. Patients with PD were scanned without interruption of the regular anti-PD medication. All patients were assessed with the Unified Parkinson Disease Rating Scale once before surgery and again immediately before the PET scan. This study followed the guidelines for research with human subjects established by our Institutional Review Board and all subjects gave written informed consent. Demographic and clinical data are shown in Table 1.

DBS and the experimental task

As a provocation task, patients performed a sequential finger-to-thumb opposition task using both hands by sequentially matching the thumb to the four other fingers of each hand, with an average frequency of 1.5 actions per second. This task has routinely been used to evaluate severity of PD symptoms especially in bradykinesia, which appears to be highly improved due to DBS in PD. We allowed slight individual differences in motor performance depending on the patient's status. However, patients were instructed to maintain a similar level of motor performance in the DBS-On and DBS-Off states, which was confirmed during the experiments. In the resting state, patients lay quietly without moving. PET scans started one minute after each patient's task was performed.

Four PET scans were acquired in the following order: resting state with DBS-On, task state with DBS-On, resting

Table 1. Demographic Data of the Study Patients

Case	Sex	Age1	Age2	SD	FUD	Preoperative state								At scan							
						H&Y	UPDRS					LED	H&Y	UPDRS						LED
							I	II	IIO	III	IIIO	IV			I	II	IIO	III	IIIO	IV	
1	M	40	46	8	76	4	3	9	15	23	53	7	700	3	3	11	11	15	15	7	950
2	F	65	67	6	18	2	3	2	12	9	30	8	1000	2	2	6	12	9	17	4	450
3	M	63	64	5	14	2.5	0	5	18	12	40	3	450	2	2	6	7	11	23	0	150
4	F	65	66	9	8	2.5	1	5	8	26	48	4	540	3	0	8	12	20	20	2	380
5	M	57	58	14	9	3	2	11	22	15	47	11	1200	2	3	5	8	5	9	7	380
6	F	48	52	8	48	3	6	8	30	12	40	19	300	3	5	21	25	16	19	10	0
7	F	52	56	14	34	5	8	12	32	21	44	8	1520	3	8	22	29	19	21	7	1140
8	F	60	64	8	48	2.5	2	22	28	20	48	12	800	2.5	2	20	23	18	21	8	940
9	M	62	64	11	24	2.5	7	14	24	16	47	7	1250	2	7	12	22	14	44	6	1550
10	F	69	73	8	49	2	2	4	14	8	26	7	900	3	3	9	20	21	24	6	685
Mean		58.1	61.0	9.1	32.8	2.9	3.4	9.2	20.3	16.2	42.3	8.6	866.0	2.6	3.5	12.0	16.9	14.8	21.3	5.7	662.5

Age1, age at surgery (years); Age2, age at scan (years); SD, symptom duration (years); FUD, follow-up duration (months); H&Y, Hoehn & Yahr; UPDRS, Unified Parkinson Disease Rating Scale; IIO, UPDRS part II without medication; IIIO, UPDRS part III without medication; LED, Levodopa equivalent dose (mg/day); M, male; F, female.

state with DBS-Off and task state with DBS-Off. Task and resting state scans for each DBS condition were separated by 15 minute intervals to allow radioactive levels to return to baseline. The DBS-On series was followed by a one-hour interval of rest outside the scanner before beginning the DBS-Off series. The stimulator was set to each subject's clinically optimal voltage based on empirical testing performed after surgery. The body and hands were restrained with belts to minimize motion, and patient status and motor performance were monitored by video during the scans. The motor performances of five of the ten patients were recorded with a video camera.

Image acquisition and image processing

Regional cerebral blood flow (rCBF) PET scans were obtained with a Philips GEMINI PET/CT scanner (Cleveland, OH, USA). For each scan, the patient received a bolus injection of 370 MBq of [^{15}O]H_2O into the antecubital vein in the left forearm through an indwelling catheter. PET data were collected over 120 seconds. Images were reconstructed based on a time-activity curve using 20–120 second intervals. Correction for tissue attenuation was based on data from low dose computed tomography transmission measurements, performed with a 140-kV, 40-mAs/slice. The acquired images were attenuation-corrected and reconstructed using the row-action maximum likelihood algorithm (3D-RAMLA).

Spatial preprocessing and statistical analysis were performed using SPM8 (University College of London, UK).[16] All reconstructed images were transformed into a standard Montreal Neurological Institute stereotactic anatomical space using nonlinear transformation of each image to a group template, which was generated by averaging all PET images after nonlinearly transforming them to the statistical parametric mapping (SPM) PET template space. Spatially normalized images were smoothed by a Gaussian filter with a kernel size of the full-width-half-maximum of 10×10×10 mm^3. All rCBF radioactivities were scaled proportional to total brain radioactivity to adjust for any global uptake variability between individuals.

Statistical parametric mapping (SPM) of rCBF changes

To investigate regional rCBF changes due to DBS and task performance, as a reference for ICA analysis, we applied two-way repeated measures ANOVA factoring DBS-On versus DBS-Off and finger-to-thumb opposition task versus resting state. Paired t-tests compared the rCBF at each vox-

el during the finger-to-thumb opposition task with corresponding values during the resting state for both DBS-On and DBS-Off. The significance threshold for the clusters was defined as an uncorrected p-value<0.005 for a cluster containing at least 227 contiguous voxels, which is equivalent to the p<0.05 criteria when corrected by cluster level for multiple comparisons, as estimated by 10000 Monte Carlo simulations.[17]

ICA of cross-sectional PET data

To examine alterations in functional networks, we used a cross-sectional ICA modified from that in our previous study.[12] For each PET image [total number M=40, i.e., 10 subjects×2 DBS conditions (On versus Off)×2 task conditions (task versus rest)], we extracted a vector of rCBFs at the voxels within the gray matter (total number of voxels, K=18323), which was defined by SPM *a priori* maps. All vectors from the M PET images were concatenated to a matrix x, which was decomposed into an independent component matrix s and a mixing matrix A using an ICA algorithm. The matrix sizes of x, s and A were (M×K), (N×K) and (M×N).

For each voxel, a vector of i-th PET image x_i can be composed of N independent components (IC) s_j, j=1,..N, as below,

$$x_i=\sum_{j=1}^{N} a_{ij}s_j,\ i=1,....,M$$

where the weight aij indicates the contribution of source s_j to compose x_i. This can be rewritten as,

$$x=[x_1,\cdots, x_M]^T=A[s_1,\cdots, s_N]^T=As$$

where x_i is a vector of the i-th PET image, s_i is a j-th IC, and A is a M×N mixing matrix composed of weight elements a_{ij}. For this study, we assumed the number of ICs (N) equaled the number of PET images (M), i.e., N=M. The mixing matrix A can be estimated using ICA algorithms, which maximize the mutual independency between the estimated functional components. To reliably estimate the functional components, we followed an ICASSO framework[18] using FastICA.[19] In this ICASSO framework, we ran FastICA 50 times with random initial values. From the pool of components driven at each run, ICASSO searches cluster centroids by computing hierarchical clustering according to the dissimilarities among components using average-linkage strategy. These cluster centroids are considered more reliable estimates for independent component.[18]

The mixing matrix A, driven by ICA algorithms, carries information on the contribution of each independent component to a measured PET image. For the weight element a_{ij} and for the j-th IC (j=1,.., M) to the i-th PET image (i=1,.., M), we conducted two-way repeated measures ANOVA with the factors: DBS condition (DBS-On versus DBS-Off) and task condition (finger-to-thumb opposition task versus rest).

RESULTS

According to the visual analysis of the recorded videos of the five patients, there was no significant difference in the motor performances between DBS-On (mean 1.57 trials/sec, ranges 1.0–2.0 trials/sec) and DBS-Off (mean 1.48 trials/sec, ranges 1.0–2.0 trials/sec) (p=0.37).

Task-induced rCBF changes during DBS-On and DBS-Off

The most significant effects from the finger-to-thumb opposition task were found in the bilateral primary sensorimotor cortex, supplementary motor area (SMA) and cerebellum for increased activation and the left middle temporal gyrus and right occipital cortex for decreased activation (Fig. 1A). We observed a tendency of increased rCBF due to DBS (if not satisfying the cluster level correction criteria p<0.05) in the right precuneus, right globus pallidum and bilateral cerebellum, while rCBF decreased in the bilateral SMA, right superior frontal gyrus, right lower precentral gyrus, thalamus and midbrain (Fig. 1B).

The activation patterns of the DBS-Off and DBS-On states differed slightly from each other. During the DBS-Off state, the finger-to-thumb opposition task activated the bilateral sensorimotor cortex, left cerebellum, and right SMA, while deactivating the right precuneus and left inferior temporal gyrus (Fig. 1C). Activation in the DBS-On state was found in the bilateral sensorimotor cortex, cerebellum and cingulate gyrus, while there was deactivation in the parahippocampal gyrus at the same time (Fig. 1D). SPM results are summarized in Table 2.

Alteration of functional networks in the ICA analysis

Fig. 2 illustrates the functional components corresponding to the task effect, DBS effect, effect of task and DBS interaction, and task performance during DBS-On and DBS-Off. Clusters in each component indicate that they were functionally connected with one another. During the DBS-On state, IC25 was the only network showing a task effect

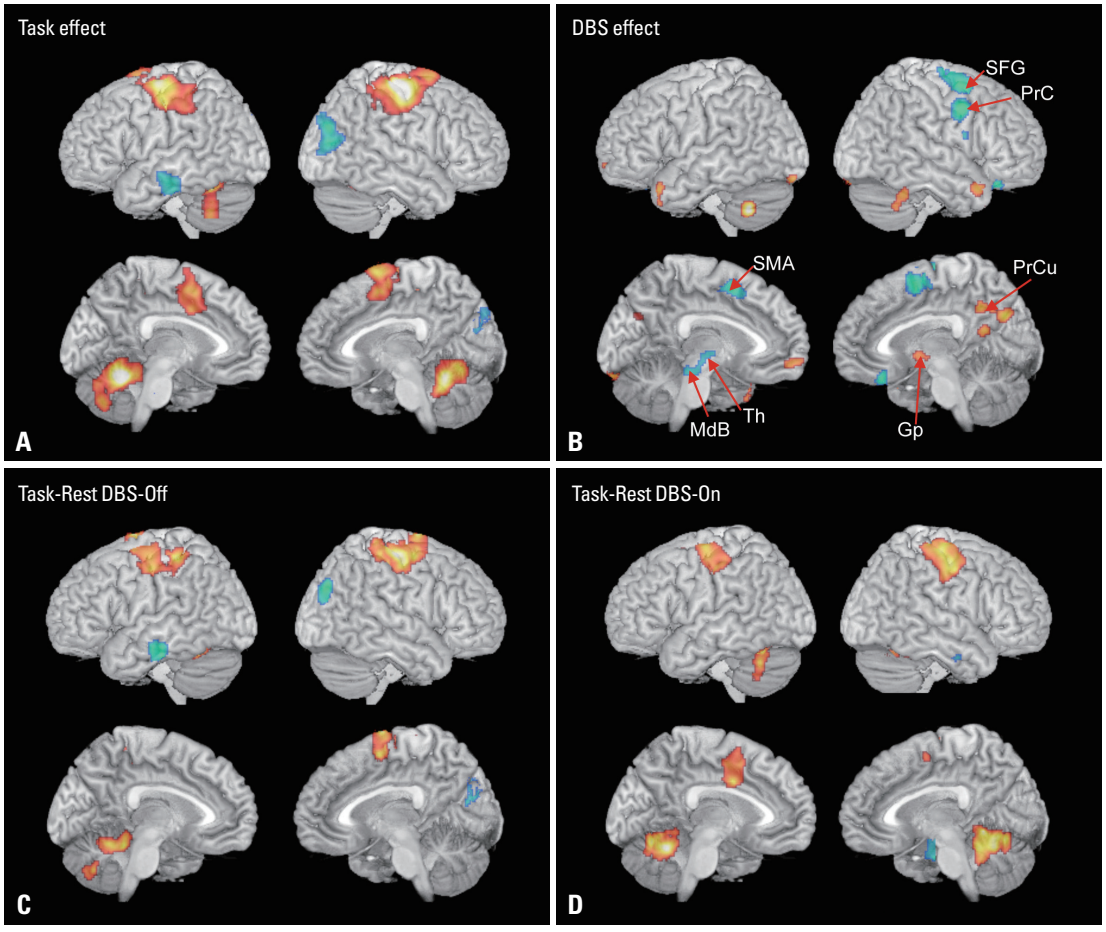

Fig. 1. SPM results of rCBF changes in patients with PD. (A) A map of significant task effects [rCBF increase (red) and decrease (blue) during the finger-to-thumb opposition task versus rest]. (B) A map of significant DBS effects [increased (red) and decreased (blue) rCBF regions during DBS-On versus DBS-Off]. The rCBF during the finger-to-thumb opposition task was compared to rCBF in the resting state with (C) DBS-Off and (D) DBS-On. Blue shows decreased rCBF and red shows increased rCBF during DBS-On versus DBS-Off. An uncorrected $p<0.005$, cluster size >227 voxels (1816 mm^3), corresponding to corrected $p<0.05$ in the cluster level by Monte Carlo simulation [except for B, uncorrected $p<0.005$, cluster size >35 voxels (280 mm^3)] are displayed. Gp, globus pallidum; MdB, midbrain; PrC, precentral gyrus; PrCu, precuneus; SMA, supplementary motor area; SFG, superior frontal gyrus; Th, thalamus; SPM, statistical parametric mapping; rCBF, regional cerebral blood flow; PD, Parkinson's disease.

(p=0.0003). The components of DBS effects were found at IC4 (p=0.037), IC6 (p=0.039), IC9 (p=0.047), IC25 (p=0.038), and IC40 (p=0.049). Interaction between task and DBS was found at IC8 (p=0.017).

In the DBS-Off state, IC25 (p=0.0007) and IC16 (p=0.030) were involved in task performance. The DBS-On state recruited networks IC25 (p=0.0013) and IC40 (p=0.046) for motor performance. IC8 (p=0.031), IC14 (p=0.017), IC25 (p=0.048), and IC40 (p=0.005) showed increased involvement in the DBS-Off resting state compared to the DBS-On resting state.

IC25 included the sensorimotor areas, premotor area and cerebellum. This component was affected by the DBS, i.e., the DBS decreased the involvement of IC25. IC9 is composed of the in-phased middle frontal gyrus, posterior cerebellum, medial frontal gyrus and left posterior cingulate cortex with anti-phased thalamus and putamen. IC6 is a network of the paracentral gyrus, SMA, precentral gyrus and left globus pallidus. IC4 is a component of the midbrain, pons and the anterior cerebellum. IC40 includes the cingulate gyrus, precuneus, cuneus, and inferior temporal gyrus with anti-phased right paracentral gyrus, frontal gyrus, left cuneus, and cerebellum. IC8 is a network of the lower precentral gyrus, inferior frontal gyrus, premotor area, posterior cingulate cortex, and cuneus with anti-phased precuneus, postcentral gyrus, superior frontal gyrus and medial frontal cortex. IC14 is composed of the SMA and superior and middle frontal cortex, left precentral gyrus, left lingual gyrus, right precuneus with the anti-phased inferior and middle frontal cortex, inferior temporal gyrus, right parietal cortex and right caudate. IC16 is a map of the paracentral gyrus, middle frontal gyrus and right precentral gyrus with the anti-

Table 2. Statistical Parametric Maps of Activation

Location	BA	k	Z*	MNI		
				X	Y	Z
Task effects						
Right pre & postcentral gyrus	4/3	4471	6.49	44	-20	60
Right supplementary motor area	6	-	4.32	12	4	68
Left supplementary motor area	6	-	4.07	0	2	52
Left cerebellar culmen		3488	6.38	-16	-54	-22
Right cerebellar culmen		-	5.10	14	-54	-20
Left precentral gyrus	4/6	2374	5.44	-40	-12	64
Left postcentral gyrus	40	-	3.66	-38	-38	56
Right superior occipital gyrus	19	710	-4.10	30	-80	26
Left middle temporal gyrus	21	388	-3.67	-62	-22	-20
DBS effects						
Left cerebellar tonsil		102	4.65	-54	-56	-44
Right cerebellar culmen		94	3.09	46	-48	-32
Right cuneus/precuneus	7/31	158	3.53	4	-72	30
Right precuneus	31	-	3.22	6	-52	38
Right globus pallidum+		35	2.84	18	2	-2
Right precentral gyrus	6	338	-4.64	48	2	40
Right superior frontal gyrus	6	570	-4.00	24	0	56
Left supplementary motor area	6	298	-3.66	-4	8	52
Right supplementary motor area	6	-	-2.78	2	-6	54
Left midbrain+		82	-2.91	-2	-28	-16
Left thalamus+		-	-2.83	-4	-12	-2
Task effect with DBS-Off						
Right post & precentral gyrus	3/4	1941	4.88	48	-20	60
Right superior frontal gyrus/SMA	6	-	4.48	14	-2	76
Left post & precentral gyrus	40/4	1054	4.24	-34	-38	56
Left cerebellar culmen		674	4.18	-14	-42	-20
Right precuneus/cuneus	19/18	264	-4.20	30	-80	32
Left inferior temporal gyrus	20	271	-3.68	-60	-26	-28
Task effect with DBS-On						
Left cerebellar culmen		2499	4.95	-18	-56	-22
Right cerebellar culmen		-	4.64	12	-50	-8
Right pre & postcentral gyrus	4/3	1722	4.27	46	-14	50
Left middle cingulate gyrus	24	426	4.05	-8	0	34
Left pre & postcentral gyrus	6/4/2	941	3.92	-40	-14	64
Right parahippocampal gyrus	35	533	-4.54	26	-20	-22

BA, Brodmann area; k, cluster size; MNI, Montreal Neurological Institute; DBS, deep brain stimulation; SMA, supplementary motor area.
An uncorrected $p<0.005$, cluster size >227 voxels (1816 mm^3), corresponding to corrected $p<0.05$ in the cluster level by Monte Carlo simulation was applied except for DBS effects. DBS effect was presented with a lower threshold, an uncorrected threshold $p<0.005$, cluster size >30 voxels (240 mm^3), to include subcortical regions marked with +.
*Positive Z indicates increased area and negative indicates decreased area.

phased left superior temporal gyrus, left inferior frontal gyrus, left putamen, left parahippocampal gyrus and pons.

DISCUSSION

The network abnormalities in PD have previously been reflected in the altered spatial covariance pattern of regional resting state PET data[20-23] and in the abnormal functional connectivity in resting state fMRI data.[5,6] Despite extensive researches on the network abnormality in PD, few studies have been conducted to examine how STN-DBS restores abnormal networks in PD, especially motor networks. In the current study, we investigated DBS-induced network changes of PD during a motor task using cross-sectional PET ICA.

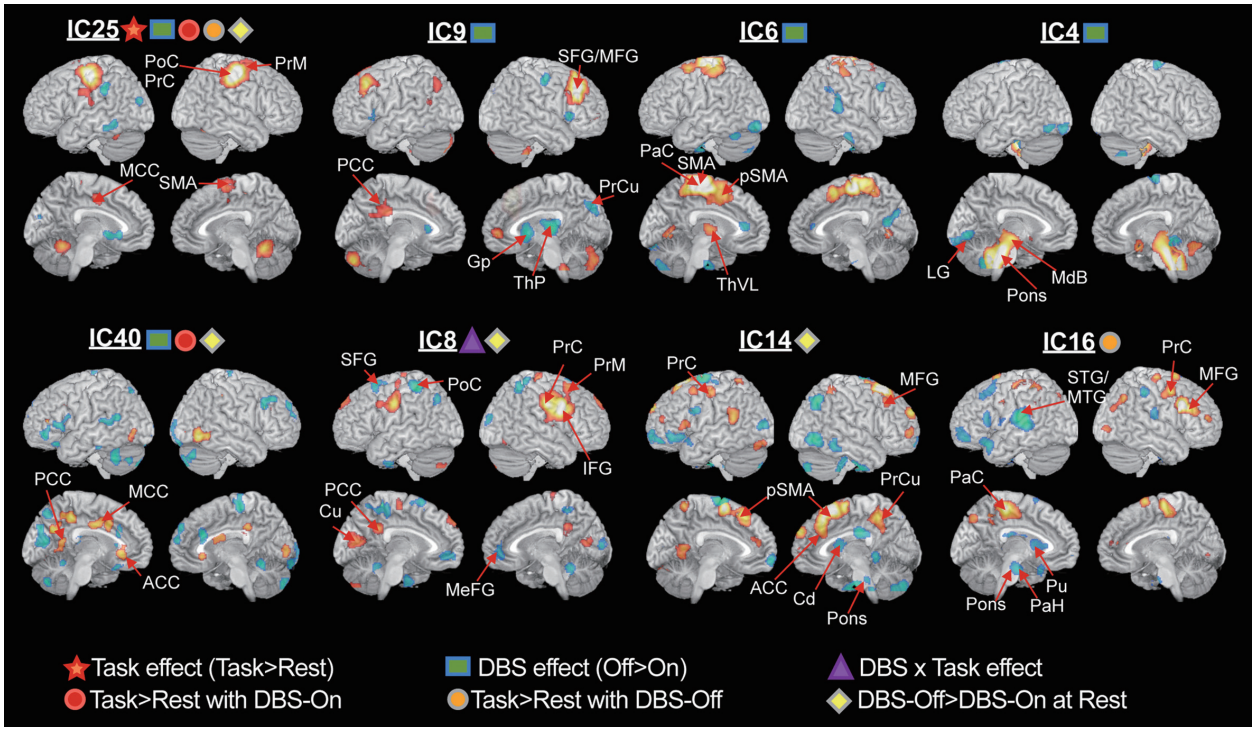

Fig. 2. Functional components for task performance with DBS-On and DBS-Off. Results from the repeated measures ANOVA of the independent components (ICs) with weights for significant task effect, DBS effect and task×DBS interaction, task induced changes according to the paired t-test during DBS-On and DBS-Off and the difference between DBS-On and DBS-Off during the resting state (p<0.05) are displayed. Voxel intensities at each IC component were Z-transformed, and clusters with Z>2 or Z<-2, cluster size >100 voxels are displayed. The main task effect was found in IC25. DBS effect was found in IC25, IC9, IC6, IC4, and IC40. DBS and task interaction were found in IC8. A task-induced increase was found in IC40 for DBS-On and IC16 for DBS-Off. Reduced involvement due to DBS during the resting state was found in IC8 and IC14. Note that red and blue colors indicate anti-phase subregions in a network. ACC, anterior cigulate cortex; Cd, caudate; Cu, cuneus; Gp, globlus pallidum; LG, lingual gyrus; MCC, middle cingulate cortex; MdB, midbrain; MeFG, medial frontal gyrus; MFG, middle frontal gyrus; MTG, middle temporal gyrus; PaC, paracentral gyrus; PaH, parahippocampal gyrus; PCC, postcentral cortex; PoC, postcentral gyrus; PrC, precentral gyrus; PrM, premotor area; PrCu, precuneus; pSMA, pre supplementary motor area; Pu, putamen; SFG, superior frontal gyrus; SMA, supplementary motor area; STG, superior temporal gyrus; ThP, thalamus pulvinar; ThVL, ventrolateral thalamus; DBS, deep brain stimulation; IFG, inferior frontal gyrus; ANOVA, analysis of variance.

Network perspective in understanding STN-DBS mechanism

The current cross-sectional ICA method is based on a connectionist view to understand the STN-DBS mechanism, which matches the network properties of the STN. While stimulation of the STN may affect multiple pathways because of its broad connectivity, STN stimulation may also block information flow through the STN, potentially preventing propagation of aberrant signals in disease.[24] The network complexity of the STN involvement leads to difficulty in identifying a specific region of DBS action. Furthermore, understanding motor-task related mechanism of DBS in terms of regional activities is more difficult as task performance itself recruits complex circuitry. Therefore, it is reasonable to assume that the modulation of STN-DBS may occur as a network for the current sequential finger-to-thumb opposition task. This network perspective provides the rationale for functional connectivity analysis using cross-sectional ICA of PET.

Network analysis and univariate subtraction method

In the current study, ICA blindly decomposed functional components corresponding to results detected in the SPM analysis (Fig. 1). In particular, the sensorimotor network (IC25) in the ICA results (Fig. 2), in which the weight showed a significant task effect, was similar to the SPM result for task effect (Fig. 1A) and task-induced increased activation in the DBS-Off and DBS-On states (Fig. 1C and D). However, we did not find a direct functional component corresponding to the SPM result of the DBS effect (Fig. 1B). Repeated measures of ANOVA of ICA weights suggested that the DBS effect in Fig. 1B may not be a single network but a mixture of multiple spatially independent networks, i.e., IC6, IC9, and IC25 for the right precentral gyrus and premotor area, and IC4 for the midbrain.

STN-DBS effects on the Parkinson's motor networks

Although some controversy exists among previous studies,[25-28] STN-DBS does suppress hyperactive cortical lobes,

such as the premotor areas and anterior cerebellum, while facilitating hypoactive regions, such as the globus pallidum/putamen, temporal gyrus and occipital gyrus. Functional components of IC25, IC9, IC6, and IC40 show a grossly consistent pattern with previous studies of PD patients, in that STN-DBS suppressed the precentral gyrus (IC25), SMA (IC25, IC6), premotor area (IC25), and cingulate (IC40), while activating the putamen (IC9), regardless of task performance or resting state.

The network difference between DBS-On and DBS-Off during motor performance is displayed in IC16 and IC40. The difference exists in the involvement of the right premotor, middle frontal gyrus and lateral parietal lobe during the DBS-Off state, which was reduced due to STN-DBS. This finding is roughly consistent with the study of Samuel, et al.,[2] who showed hyperactivity in the lateral premotor and parietal cortex and hypoactivity in the SMA of patients with PD during sequential and bimanual movement. IC40 is also a plausible network comprised of the anterior, middle and posterior cingulate cortices, which are interconnected with each other by cingulum bundle fibers. The reduced rCBF in the cingulate network due to STN-DBS (IC40) was also found in a previous study.[27]

An important advantage of ICA is its ability to provide information regarding brain networks in PD and their changes due to STN-DBS. In agreement with the well-known connectivity of the thalamus, i.e., from the pulvinar to the posterior association cortex and from the ventrolateral subnuclei to the motor and somatosensory cortices, we observed co-activation between the pulvinar of the thalamus and the precuneus in IC9 and between the ventrolateral thalamus and the paracentral cortex-SMA in IC6. STN-DBS increased the pulvinar activity together with the precuneus and the putamen in IC9, while reducing both ventrolateral thalamic activity and motor cortical activities in IC6. The decreased blood flow at the ventrolateral thalamus due to STN-DBS was previously observed.[26,27] The increased rCBF due to STN-DBS at the thalamic pulvinar in IC9 is consistent with the result of Hershey, et al.[25] However, STN-DBS effects on rCBF changes in the ventrolateral thalamus in PD are still controversial as other studies showed increased blood flow or metabolism at the thalamus.[20,28,29]

Despite this controversy, the interpretations are commonly based on the classical model of the basal ganglia-thalamocortical network[30] to explain the different rCBF changes at the thalamus due to STN-DBS. According to the classical model of PD,[31,32] the increased net output from the STN-DBS[25] excites the internal globus pallidus, which has an increased inhibitory drive to the thalamus that reduces the excitatory thalamic drive to the cerebral cortex. To explain the increased thalamic rCBF due to the STN-DBS, one may attribute these findings to the pallidal inhibitory connection that is highly active at the terminal synapse located in the thalamus, thereby inducing increased rCBFs at the thalamus. On the contrary, the decreased thalamic rCBF due to STN-DBS can be explained by the relationship between the inhibitory neurons and rCBF changes[27] since GABA-ergic inhibition reduces blood flow to the target area.[33-36] This controversial interpretation may be attributable not to the basal ganglia-thalamo-cortical network problem but possibly to the neuro-vascular coupling problem, i.e., what the rCBF reflects in association with neural activity. Geday, et al.[27] discussed that suppressed ventrolateral thalamic rCBFs decreased cortical rCBFs due to STN-DBS, similar to our present finding, which fits the basal ganglia-thalamo-cortical network model more accurately than the theory that increased thalamic rCBFs.

Intrinsic motor networks of PD in independent components

Based on the distributed activity pattern within a functional component, we can infer intrinsic brain networks in PD. The globus pallidum showed an anti-phased co-activation with the cerebellum, premotor and dorsolateral prefrontal cortex but no apparent co-activation with the motor cortex in IC9. The anti-phase co-activation between the globus pallidum and the cerebellum without a significant co-activation with the motor cortex is consistent with a resting-state fMRI study of patients with PD.[37]

The anterior putamen showed an anti-phased connection with the premotor and the precental gyrus, however, an in-phased connection with the superior/middle temporal gyrus, middle frontal cortex and pons in IC16. The in-phased connection from the anterior putamen is again consistent with a study of Helmich, et al.[38] which showed functional connectivity between the anterior putamen and the middle frontal gyrus, middle temporal gyrus and mesencephalon in both patients with PD and healthy controls using resting-state fMRIs. Both the globus pallidum and putamen had an anti-phased connection with the superior and middle frontal cortices in IC9 and IC16.

The anti-phase connection between the putamen/globus pallidum and cortical regions and the in-phase connection between the ventrolateral thalamus and motor cortical re-

gions, found in IC16 and IC9, are consistent with a model of the basal ganglia-thalamo-cortical network developed by Alexander, et al.[39] Although the weights of IC9 and IC16 differed according to conditions, e.g., IC9 was suppressed by STN-DBS and IC16 was significantly involved in a motor task during DBS-Off, the spatial components were derived from all the PET data of patients regardless of tasks and DBS states. Therefore, the spatial patterns of ICs reflect intrinsic network properties in patients with PD. This is partly supported by fMRI studies showing that task-activated networks are embedded in spontaneous activities.[40,41]

In summary, the functional components blindly decomposed using a cross-sectional ICA have plausible bases in previous studies and provides how DBS changes patterns of functional association among brain regions otherwise unresolved in the subtraction approach.

Cross-sectional ICA for network analysis using static PET

The usefulness of the cross-sectional ICA was previously demonstrated in the identification of group-specific spatial patterns of gray matter in the voxel-based morphometry[42] and in the decomposition of functional networks from cross-sectional [^{18}F]fluoro-deoxy-glucose PET comparable to networks found in the resting state fMRI.[43] Since voxels that convey similar information are clustered into a single independent component, an independent component from ICA represents a tight association between brain regions within the component and can be regarded as a "network".[42]

A multivariate analysis using ICA has advantages over univariate subtraction methods in providing network information, especially in brain research where each region works in collaboration with other inter-connected regions.[44] In contrast to PCA-based methods, ICA is designed to find independent functional components by maximizing the statistical independence of the estimated components. The current study showed that cross-sectional ICA is highly useful in identifying functional components for network analysis in addition to carrying univariate activity information.

Limitations of experiment

In terms of experiment and data interpretation, this study has several limitations. The relatively small number of patients may explain the low statistical power in the comparison of weights. However, each IC component pattern was derived from a group of subjects and carries information on common brain networks embedded in patients with PD, regardless of statistical significance of its involvement (i.e., weight) in a certain task, DBS effect or else.

We did not conduct DBS-Off scanning before DBS-On because all of the patients found it extremely difficult to perform the motor task without DBS and because we considered that the compound effects such as learning or fatigue might not be significant due to the simplicity of the task and sufficient resting interval between scans.

We were also unable to wait for the brain to completely return to the baseline state before conducting the task with DBS-Off. This was because the patients could carry out the task for only a limited time after DBS-Off. Therefore, we cannot disregard the possibility of transient DBS-abstinent effects in brain network modification. Nevertheless, the transient effects could be explained using the alteration of weights for fixed spatial components according to current ICA model.

The relatively short interval between the second motor performance task and DBS-Off start time may explain no significant task performance decrease (from visual analysis of available five video-recordings) in the patients after DBS-Off. Indeed, the time course of behaviour changes after DBS-Off has not been clearly understood. However, we found significant alterations in the brain network usages reflected in rCBF synchrony. The significant alteration in the neural level may indicate faster or more sensitive changes in the neural networks than those in behaviours. Alterations in the neural level without significant motor performance reduction may be interpreted as hierarchical reconfiguration of brain networks to compensate the lack of normal modulations (by STN-DBS) to achieve the required motor function using available resources. In the network perspective, it is possible to achieve a given task using different network configurations.[45] However, this is simply a speculation that requires more concrete evidences.

In the current study, we evaluated the DBS effects on patients with PD. However, network analysis of motor performance PET data from PD patients without DBS, different subtypes of PD with DBS and healthy subjects would be very important in understanding DBS effects in detail, which is left for further investigations.

We conclude from our study that bilateral STN-DBS changes not only regional activities but also abnormal motor networks in patients with PD. This study also suggests that ICA of cross-sectional PET data is useful for revealing network alterations, which cannot be detected using the subtraction method.

ACKNOWLEDGEMENTS

This research was supported by the Brain Research Program of the National Research Foundation of Korea, funded by the Ministry of Science, ICT & Future Planning (2010-0018839). The authors thank Dr. Lee Phil Hyu for his helpful advice regarding the interpretation of the data.

REFERENCES

1. Turner RS, Grafton ST, McIntosh AR, DeLong MR, Hoffman JM. The functional anatomy of parkinsonian bradykinesia. Neuroimage 2003;19:163-79.
2. Samuel M, Ceballos-Baumann AO, Blin J, Uema T, Boecker H, Passingham RE, et al. Evidence for lateral premotor and parietal overactivity in Parkinson's disease during sequential and bimanual movements. A PET study. Brain 1997;120(Pt 6):963-76.
3. Rascol O, Sabatini U, Fabre N, Brefel C, Loubinoux I, Celsis P, et al. The ipsilateral cerebellar hemisphere is overactive during hand movements in akinetic parkinsonian patients. Brain 1997;120(Pt 1):103-10.
4. Grafton ST, Turner RS, Desmurget M, Bakay R, Delong M, Vitek J, et al. Normalizing motor-related brain activity: subthalamic nucleus stimulation in Parkinson disease. Neurology 2006;66:1192-9.
5. Baudrexel S, Witte T, Seifried C, von Wegner F, Beissner F, Klein JC, et al. Resting state fMRI reveals increased subthalamic nucleus-motor cortex connectivity in Parkinson's disease. Neuroimage 2011;55:1728-38.
6. Wu T, Chan P, Hallett M. Effective connectivity of neural networks in automatic movements in Parkinson's disease. Neuroimage 2010;49:2581-7.
7. Clark CM, Kessler R, Buchsbaum MS, Margolin RA, Holcomb HH. Correlational methods for determining regional coupling of cerebral glucose metabolism: a pilot study. Biol Psychiatry 1984;19:663-78.
8. Horwitz B, Duara R, Rapoport SI. Age differences in intercorrelations between regional cerebral metabolic rates for glucose. Ann Neurol 1986;19:60-7.
9. Metter EJ, Riege WH, Kuhl DE, Phelps ME. Cerebral metabolic relationships for selected brain regions in healthy adults. J Cereb Blood Flow Metab 1984;4:1-7.
10. Moeller JR, Strother SC, Sidtis JJ, Rottenberg DA. Scaled subprofile model: a statistical approach to the analysis of functional patterns in positron emission tomographic data. J Cereb Blood Flow Metab 1987;7:649-58.
11. Moeller JR, Strother SC. A regional covariance approach to the analysis of functional patterns in positron emission tomographic data. J Cereb Blood Flow Metab 1991;11:A121-35.
12. Park HJ, Kim JJ, Youn T, Lee DS, Lee MC, Kwon JS. Independent component model for cognitive functions of multiple subjects using [15O]H2O PET images. Hum Brain Mapp 2003;18:284-95.
13. Beckmann CF, DeLuca M, Devlin JT, Smith SM. Investigations into resting-state connectivity using independent component analysis. Philos Trans R Soc Lond B Biol Sci 2005;360:1001-13.
14. McKeown MJ, Sejnowski TJ. Independent component analysis of fMRI data: examining the assumptions. Hum Brain Mapp 1998;6:368-72.
15. Biswal BB, Ulmer JL. Blind source separation of multiple signal sources of fMRI data sets using independent component analysis. J Comput Assist Tomogr 1999;23:265-71.
16. Friston KJ, Holmes AP, Worsley KJ, Poline JB, Frith CD, Frackowiak RSJ. Statistical parametric maps in functional imaging: a general approach. Hum Brain Mapp 1995;2:189-210.
17. Xiong J, Gao JH, Lancaster JL, Fox PT. Clustered pixels analysis for functional MRI activation studies of the human brain. Hum Brain Mapp 1995;3:287-301.
18. Himberg J, Hyvärinen A, Esposito F. Validating the independent components of neuroimaging time series via clustering and visualization. Neuroimage 2004;22:1214-22.
19. Hyvärinen A. Fast and robust fixed-point algorithms for independent component analysis. IEEE Trans Neural Netw 1999;10:626-34.
20. Asanuma K, Tang C, Ma Y, Dhawan V, Mattis P, Edwards C, et al. Network modulation in the treatment of Parkinson's disease. Brain 2006;129(Pt 10):2667-78.
21. Lozza C, Baron JC, Eidelberg D, Mentis MJ, Carbon M, Marié RM. Executive processes in Parkinson's disease: FDG-PET and network analysis. Hum Brain Mapp 2004;22:236-45.
22. Moeller JR, Nakamura T, Mentis MJ, Dhawan V, Spetsieres P, Antonini A, et al. Reproducibility of regional metabolic covariance patterns: comparison of four populations. J Nucl Med 1999;40:1264-9.
23. Metter EJ, Riege WH, Kameyama M, Kuhl DE, Phelps ME. Cerebral metabolic relationships for selected brain regions in Alzheimer's, Huntington's, and Parkinson's diseases. J Cereb Blood Flow Metab 1984;4:500-6.
24. Perlmutter JS, Mink JW. Deep brain stimulation. Annu Rev Neurosci 2006;29:229-57.
25. Hershey T, Revilla FJ, Wernle AR, McGee-Minnich L, Antenor JV, Videen TO, et al. Cortical and subcortical blood flow effects of subthalamic nucleus stimulation in PD. Neurology 2003;61:816-21.
26. Cilia R, Marotta G, Landi A, Isaias IU, Mariani CB, Vergani F, et al. Clinical and cerebral activity changes induced by subthalamic nucleus stimulation in advanced Parkinson's disease: a prospective case-control study. Clin Neurol Neurosurg 2009;111:140-6.
27. Geday J, Østergaard K, Johnsen E, Gjedde A. STN-stimulation in Parkinson's disease restores striatal inhibition of thalamocortical projection. Hum Brain Mapp 2009;30:112-21.
28. Hilker R, Voges J, Weisenbach S, Kalbe E, Burghaus L, Ghaemi M, et al. Subthalamic nucleus stimulation restores glucose metabolism in associative and limbic cortices and in cerebellum: evidence from a FDG-PET study in advanced Parkinson's disease. J Cereb Blood Flow Metab 2004;24:7-16.
29. Karimi M, Golchin N, Tabbal SD, Hershey T, Videen TO, Wu J, et al. Subthalamic nucleus stimulation-induced regional blood flow responses correlate with improvement of motor signs in Parkinson disease. Brain 2008;131(Pt 10):2710-9.
30. Alexander GE, Crutcher MD. Functional architecture of basal ganglia circuits: neural substrates of parallel processing. Trends Neurosci 1990;13:266-71.
31. Albin RL, Young AB, Penney JB. The functional anatomy of basal ganglia disorders. Trends Neurosci 1989;12:366-75.
32. DeLong MR. Primate models of movement disorders of basal ganglia origin. Trends Neurosci 1990;13:281-5.

33. Roland PE, Friberg L. The effect of the GABA-A agonist THIP on regional cortical blood flow in humans. A new test of hemispheric dominance. J Cereb Blood Flow Metab 1988;8:314-23.
34. Takano B, Drzezga A, Peller M, Sax I, Schwaiger M, Lee L, et al. Short-term modulation of regional excitability and blood flow in human motor cortex following rapid-rate transcranial magnetic stimulation. Neuroimage 2004;23:849-59.
35. Xi ZX, Wu G, Stein EA, Li SJ. GABAergic mechanisms of heroin-induced brain activation assessed with functional MRI. Magn Reson Med 2002;48:838-43.
36. Chen Z, Silva AC, Yang J, Shen J. Elevated endogenous GABA level correlates with decreased fMRI signals in the rat brain during acute inhibition of GABA transaminase. J Neurosci Res 2005;79:383-91.
37. Yu H, Sternad D, Corcos DM, Vaillancourt DE. Role of hyperactive cerebellum and motor cortex in Parkinson's disease. Neuroimage 2007;35:222-33.
38. Helmich RC, Derikx LC, Bakker M, Scheeringa R, Bloem BR, Toni I. Spatial remapping of cortico-striatal connectivity in Parkinson's disease. Cereb Cortex 2010;20:1175-86.
39. Alexander GE, DeLong MR, Strick PL. Parallel organization of functionally segregated circuits linking basal ganglia and cortex. Annu Rev Neurosci 1986;9:357-81.
40. Xiong J, Parsons LM, Gao JH, Fox PT. Interregional connectivity to primary motor cortex revealed using MRI resting state images. Hum Brain Mapp 1999;8:151-6.
41. Smith SM, Fox PT, Miller KL, Glahn DC, Fox PM, Mackay CE, et al. Correspondence of the brain's functional architecture during activation and rest. Proc Natl Acad Sci U S A 2009;106:13040-5.
42. Xu L, Groth KM, Pearlson G, Schretlen DJ, Calhoun VD. Source-based morphometry: the use of independent component analysis to identify gray matter differences with application to schizophrenia. Hum Brain Mapp 2009;30:711-24.
43. Di X, Biswal BB; Alzheimer's Disease Neuroimaging Initiative. Metabolic brain covariant networks as revealed by FDG-PET with reference to resting-state fMRI networks. Brain Connect 2012;2:275-83.
44. Clark C, Carson R, Kessler R, Margolin R, Buchsbaum M, DeLisi L, et al. Alternative statistical models for the examination of clinical positron emission tomography/fluorodeoxyglucose data. J Cereb Blood Flow Metab 1985;5:142-50.
45. Park HJ, Friston K. Structural and functional brain networks: from connections to cognition. Science 2013;342:1238411.